Supporting Information

Synergistic Electrolyte Design for Dual-Interface Stability in Sodium-Ion Batteries

Zijuan Luo,[a] Yinxiao Cai,[a] Yanan Zhou,[a] Xing Xin,*[a] Mingjiong Zhou,*[a] Yongfeng Liu,[b] Zengxue Wu,[c] Weili Sun,[c] Lee Jonghee,[c] Kun Zheng,[d] Konrad Świerczek,[d] Snežana Papović,[e]

[a]*School of Materials Science and Chemical Engineering, Ningbo University, Ningbo 315211, China.*
[b]*School of Materials Science and Engineering, Zhejiang University, Hangzhou 310058, China.*
[c]*Ningbo Ronbay New Energy Technology Co., Ltd., Ningbo 315400, P. R. China.*
[d]*Faculty of Energy and Fuels, AGH University of Krakow, Al. A. Mickiewicza 30, 30-059 Krakow, Poland.*
[e]*Faculty of Sciences, University of Novi Sad, Novi Sad 21000, Serbia.*

Keywords: Sodium-ion batteries; electrolyte; dual-additive; SEI; CEI

E-mail: xinxing@nbu.edu.cn; zhoumingjiong@nbu.edu.cn
* Corresponding authors

1. Experimental procedures

1.1 Preparation of electrolytes.

The 1 M $NaClO_4$ in EC/DMC (1:1 vol%) electrolyte, referred to as NED, was purchased from Xiamen Chanson New Energy Co., Ltd. The electrolyte 1 M $NaClO_4$ in EC/DMC (1:1 vol%) with 2 vol% FEC was designated as NEDF, and the electrolyte 1 M $NaClO_4$ in EC/DMC (1:1 vol%) with 2 vol% FEC and 3 vol% 2-FP was designated as NEDFP. Fluoroethylene carbonate (FEC, 99%) and 2-fluoropyridine (2-FP, 98%) were obtained from Macklin. All electrolytes were prepared in an argon-filled glovebox with oxygen and moisture levels below 0.1 ppm.

1.2 Preparation of electrodes.

The $Ni_{1/3}Fe_{1/3}Mn_{1/3}(OH)_2$ precursor (purchased from GEM Co., Ltd.) was mixed with sodium carbonate (2% excess) and then calcined at 900°C for 15 hours with a heating rate of 5°C per minute. After calcination, the sample was slowly cooled to 100°C and immediately transferred to an argon-filled glovebox.

Electrochemical testing was performed using CR2032-type coin cells assembled in an argon-filled glovebox. The cathode slurry was prepared by thoroughly mixing the cathode material, conductive carbon black, and poly (vinylidene fluoride) binder (Super P/PVDF, Guangdong Canrd New Energy Technology Co., Ltd.) in a mass ratio of 80:10:10 in N-methyl-2-pyrrolidone (NMP, Aladdin). The resulting slurry was blade-coated onto aluminum foil and vacuum-dried at 110°C for 6 hours. The dried cathode sheets (Φ14 mm) had an active material loading of 2.0-2.5 mg. The cells were assembled using the prepared cathode sheet, a glass fiber separator (Whatman GF/G), a sodium metal disk (Guangdong Canrd New Energy Technology Co., Ltd.), and 0.15 mL of electrolyte. The pouch cell cores, with an N/P ratio of 1.23, were provided by Ningbo Ronbay New Energy Technology Co., Ltd.

1.3 Materials characterization and electrochemical measurement.

To analyze the surface composition and morphology of the $NaNi_{1/3}Fe_{1/3}Mn_{1/3}O_2$ (NFM) cathode material, the cycled cells were disassembled in an argon-filled glovebox to retrieve the cathode sheets. The cathodes were thoroughly washed three times with dimethyl carbonate (DMC) to remove electrolyte residues and then dried in a vacuum oven for 8 hours. The morphology of the electrodes was observed using scanning electron microscopy (SEM, Hitachi, Japan) and transmission electron microscopy (TEM, JEM2100, JEOL). The morphology of the Na was investigated by the WMJ-9590 metallographic microscope. X-ray photoelectron

spectroscopy (XPS, Thermo Scientific Nexsa) characterized the surface chemical composition with the binding energy scale calibrated primarily using the C 1s peak, referenced to the non-graphitic carbon layer at 284.8 eV. The crystal structure of the NFM after 100 cycles was determined using X-ray diffraction (XRD, D8 Advance, Bruker) with a scanning range of 10° to 70°. The NFM||Na battery was disassembled in a completely discharged state. The content of transition metal ions deposited on the surface of Na was studied through inductively coupled plasma optical emission spectroscopy (ICP-OES, Spectro ARCOS II). The activation energy was calculated using the following formula: The activation energy (E_a) at the Na-electrolyte interface is evaluated with electrochemical impedance spectroscopy (EIS) in symmetric Na||Na batteries from 293.15 to 313.15 K. It can be calculated based on the Arrhenius equation[1-4],

$$\ln(k) = \ln\left(\frac{T}{R_{res}}\right) = -\frac{E_a}{RT} + \ln A \#(1)$$

where k is the rate constant, T is the absolute temperature, R_{res} (R_{int} or R_{ct}) is the ion transfer resistance (the E_a specifically refers to the R_{int} calculation), A is the preexponential constant, E_a is the activation energy and R is the standard gas constant.

2. Calculation methods.

Simulation details: Molecular structure optimization was performed using the $DMol_3$ module in the Material Studio (MS) software. The highest occupied molecular orbital and lowest unoccupied molecular orbital energy levels of 2-FP, FEC, and the relevant carbonate-based electrolyte solvents EC and DMC were calculated accordingly. Additionally, the electrostatic potential of 2-FP and FEC molecules, as well as the binding energies between Na^+ and each solvent or additive molecule, were analyzed using density functional theory (DFT) within the $DMol_3$ module of MS. The Perdew-Burke-Ernzerhof (PBE) exchange-correlation functional within the generalized gradient approximation (GGA) was employed for molecular structure optimization. The precision was set to "fine," with all other settings kept at their default values. After structure optimization, static calculations were performed for the Na^+ complexes with 2-FP and FEC to obtain their electrostatic potentials and optimized structures.

The binding energy (E_b) is defined as follows: $E_b = E_{ion-solvent/additive} - E_{solvent/additive} - E_{ion}$, where $E_{ion-solvent/additive}$, $E_{solvent/additive}$, and E_{ion} represent the total energies of the solvent/additive-Na^+ complex, the solvent/additive molecule, and the Na^+, respectively. Based on the existing XRD standard card for metallic sodium, the adsorption of 2-FP and FEC molecules on the Na (110) surface was simulated, and DFT-optimized structures were calculated using the $DMol_3$ module. The modeling was performed on a body-centered cubic (BCC) sodium metal surface

with a 2×2×2 expanded supercell, constructing a four-layer sodium slab with a vertical vacuum region of at least 15 Å. Structure optimization was again carried out using the $DMol_3$ module. The adsorption energy (E) was defined as the difference between the total energy of the solvent molecule adsorption system (E_{total}) and the sum of the isolated solvent molecule (2-FP or FEC) and the clean Na substrate: $E = E_{total} - (E_{solvent} + E_{substrate})$, where a higher *E* value indicates stronger adsorption.

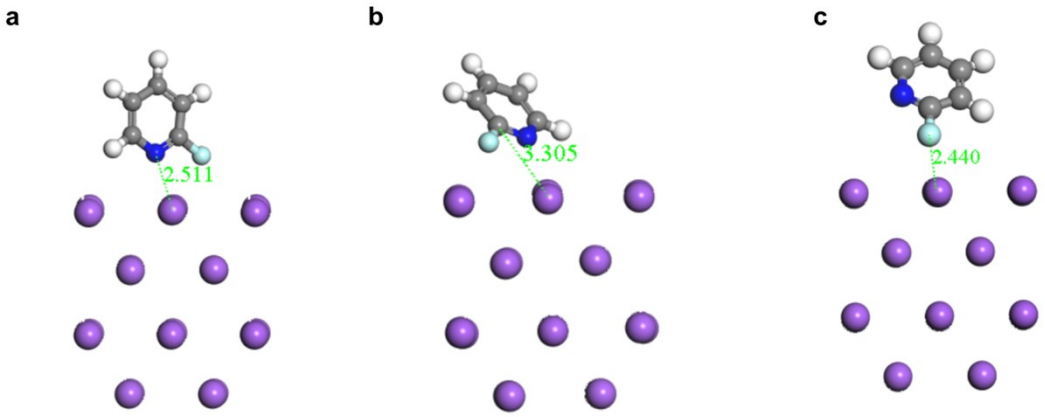

Total Energy : -2942.712 Ha > -2942.721 Ha > -2942.726 Ha

Fig. S1 The adsorption of 2-FP molecule and Na (110) simulated the state of the optimized structure and the energy of the system (a) N-terminal adsorption；(b) N, F-angle adsorption ；(c) F-terminal adsorption

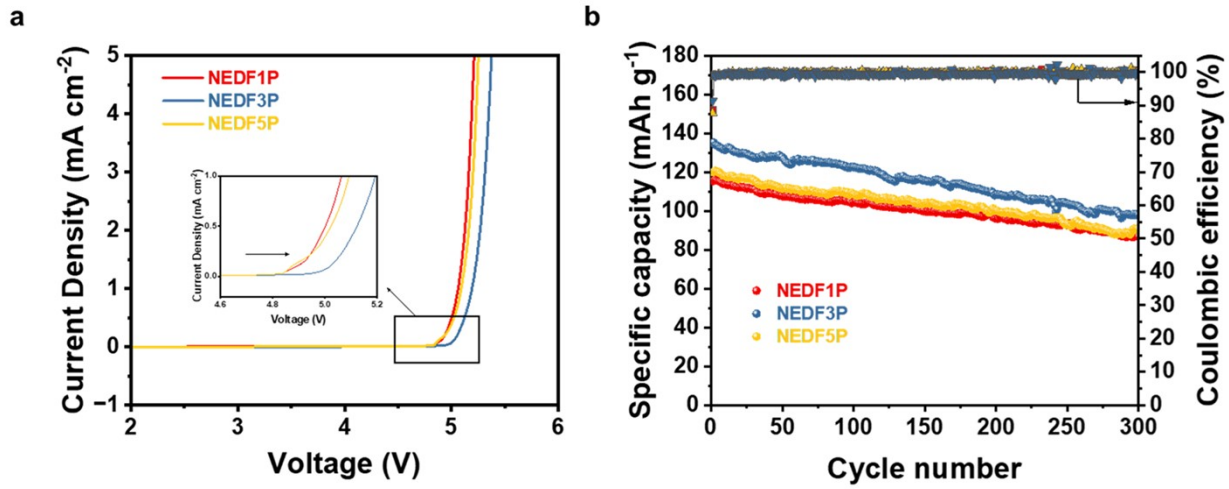

Fig. S2 (a) Linear sweep voltammetry measurement of different 2-FP contents from 2.0 to 6.0 V; (b) cycling performance and Coulombic efficiency.

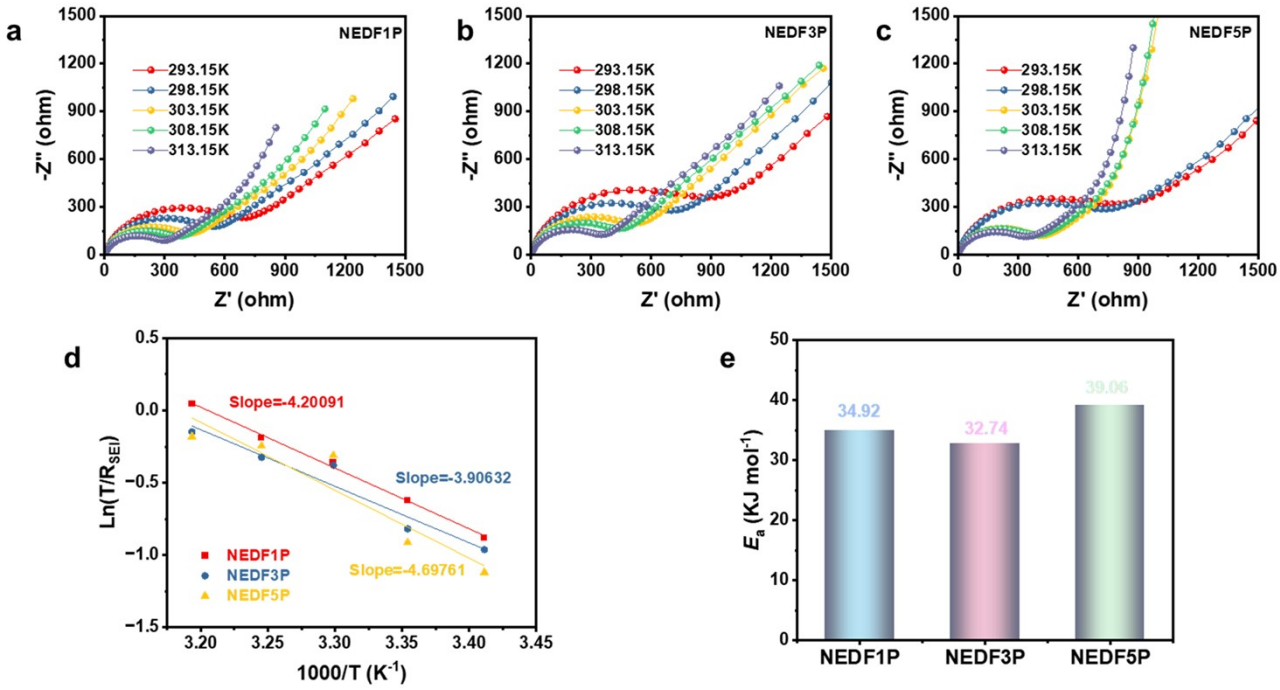

Fig. S3 Nyquist plots of symmetric at different temperatures for electrolytes with (a) 1 vol % 2-FP, (b) 3 vol % 2-FP, and (c) 5 vol % 2-FP; and Activation energy calculated by Arrhenius equation derived from Nyquist plots (d-e).

To elucidate the distinct contribution of 2-FP within the NEDFP electrolyte, diverse formulations were assessed for their electrochemical windows and performance in NFM||Na batteries. The NEDF3P formulation exhibited superior antioxidation capabilities and the broadest electrochemical window (Fig. S1a†). Electrolyte concentration variations in NFM||Na batteries were explored, identifying the optimal mix containing 2 vol % FEC and 3 vol % 2-FP (Fig. S1b†). NEDF3P demonstrated the highest initial reversible capacity at 134.9 mAh g^{-1}, compared to only 115.3 mAh g^{-1} for NEDF1P and 119.9 mAh g^{-1} for NEDF5P. Furthermore, temperature-dependent EIS (Fig. S2a-c†) elucidated the activation energies (*E*a) for Na^+ migration through the SEI, with NED3P showing a notably lower Ea of 32.47 KJ mol^{-1} against 34.92 KJ mol^{-1} and 39.06 KJ mol^{-1} for the other formulations (Fig. S2d-e†). These findings confirm that NEDFP significantly enhances interfacial transfer kinetics, establishing it as the optimal formulation: 1 M $NaClO_4$ in EC/DMC (1:1 vol %) + 2 vol % FEC + 3 vol % 2-FP.

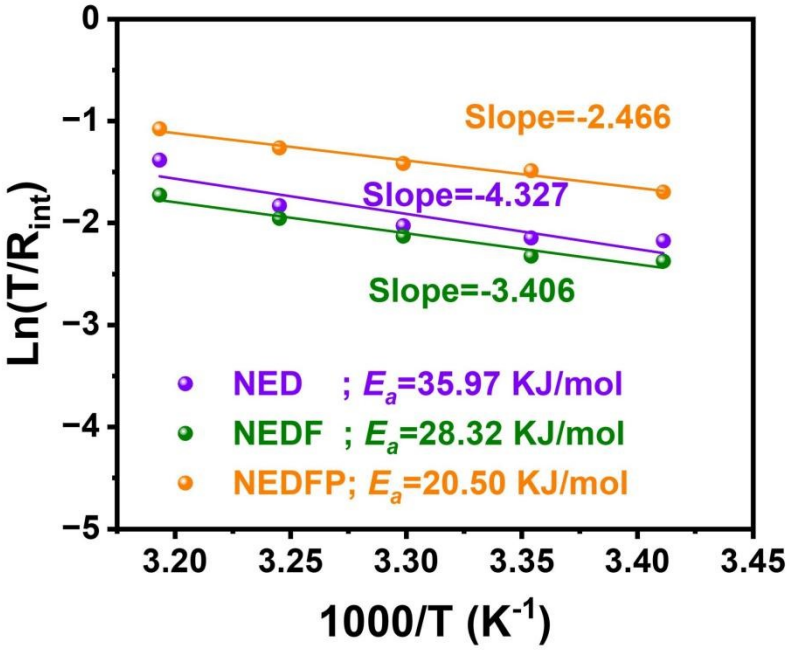

Fig. S4 The NFM||Na cells for activation energy of different electrolytes after three cycles.

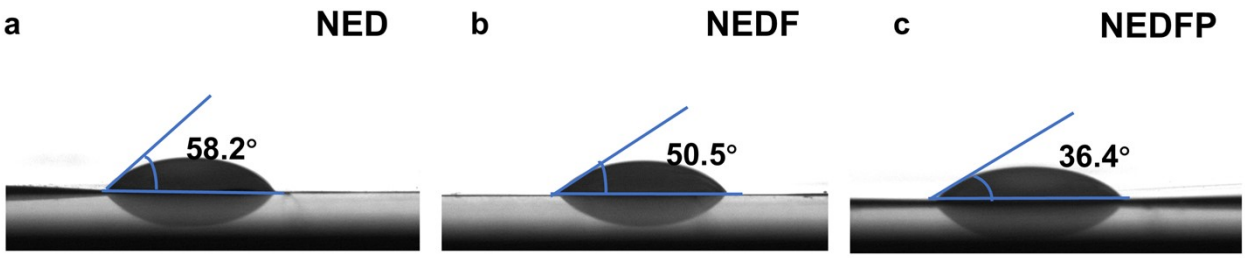

Fig. S5 Contact angles of (a) NED electrolyte, (b) NEDF electrolyte, and (c) NEDFP electrolyte.

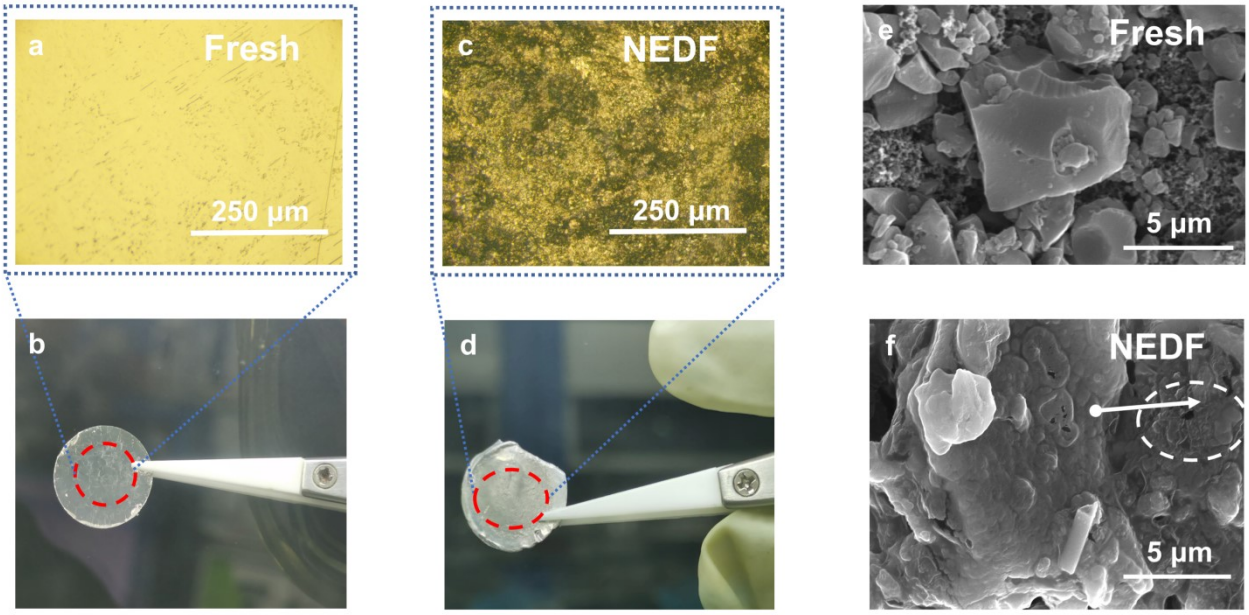

Fig. S6 Microscopic images of the surface of the Na foil (a, b) without cycling and (c, d) after cycling in NEDF electrolytes; The SEM images of (e) the fresh HC and (f) the electrodes cycled for 30th in NEDF electrolytes.

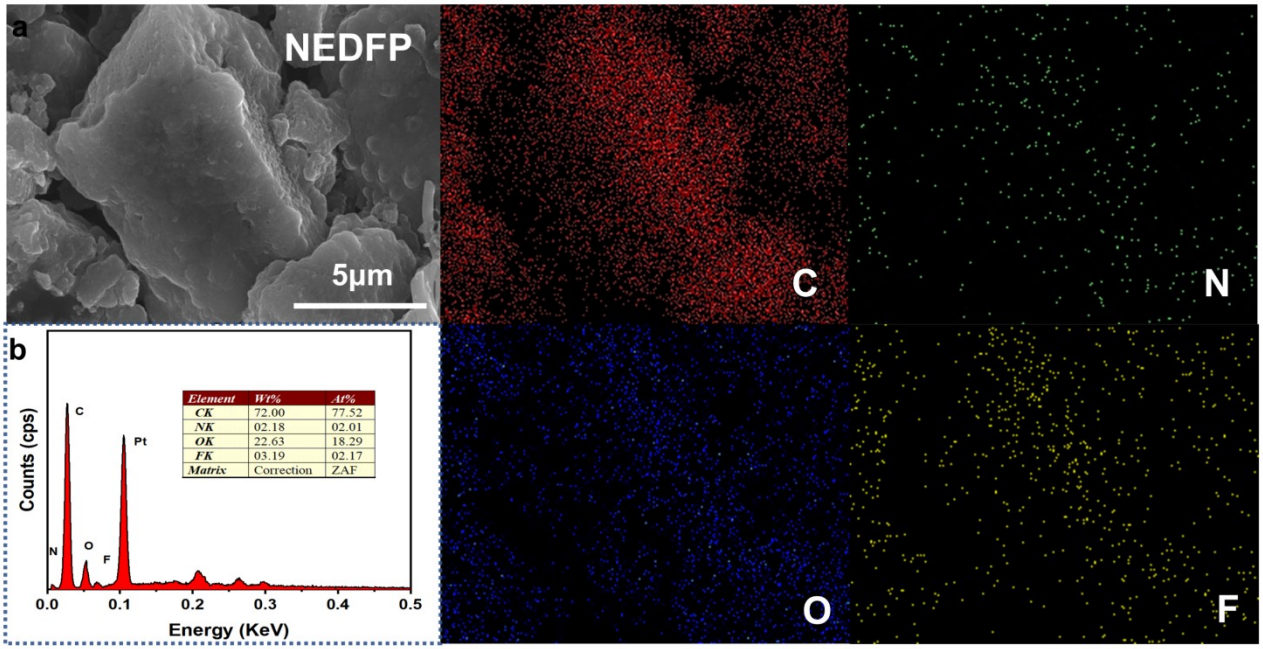

Fig. S7 SEM image of HC after 30 cycles in NEDFP electrolyte (a); and EDX mapping of different elements (b).

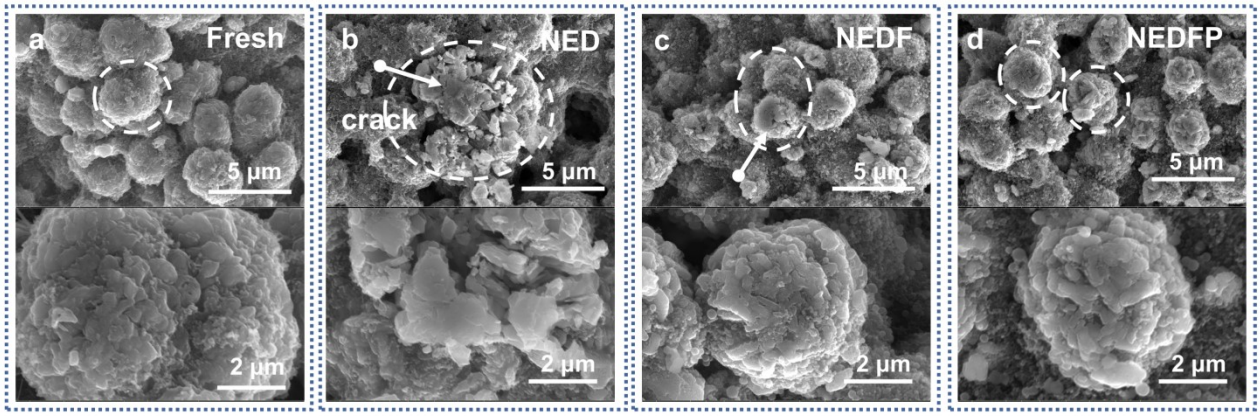

Fig. S8 The SEM images of (a) the fresh cathode and the electrodes cycled for 30th in (b) NED, (c) NEDF, and (d) NEDFP electrolytes.

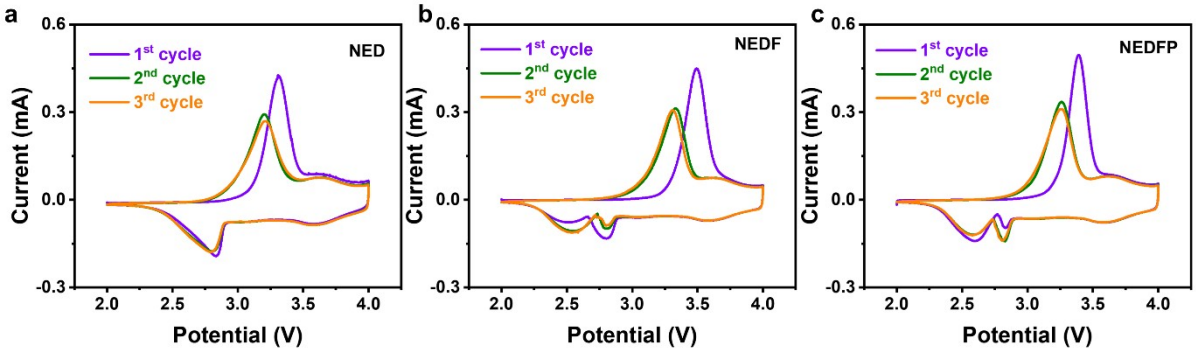

Fig. S9 The CVs of NFM||Na cells within the voltage range from 2.0 V to 4 V at 0.1 mV s^{-1} in (a) NED, (b) NEDF, and (c) NEDFP electrolytes.

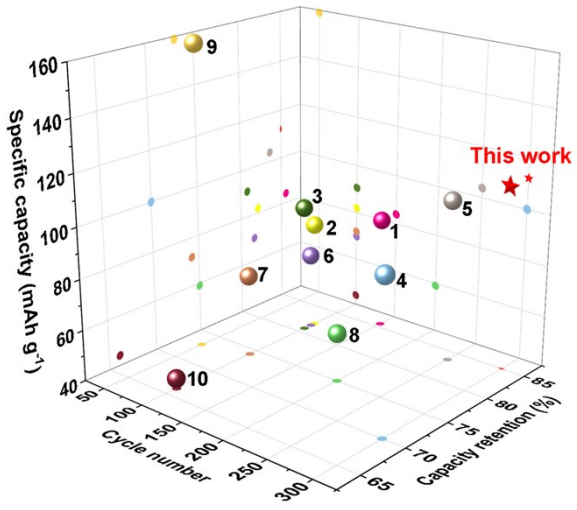

Fig. S10 Comparison of cycling performance (specific capacity vs. capacity retention) in this work and previously reported works.[1-10]

Table S1. R_s, R_{sf} and R_{ct} values for the three electrolytes at different cycle numbers.

		NED	NEDF	NEDFP
R_s Ω	1^{st}	6.0	4.4	4.3
	30^{th}	7.4	4.1	4.1
	60^{th}	6.9	4.1	4.1
	80^{th}	7.8	4.3	4.2
	100^{th}	7.9	4.1	3.9
R_{sf} Ω	1^{st}	24.3	131.8	580.6
	30^{th}	102.5	366.0	146.2
	60^{th}	114.4	150.4	126.5
	80^{th}	126.8	99.8	136.8
	100^{th}	123.3	143.6	163.0
R_{ct} Ω	1^{st}	2112	898.4	2372
	30^{th}	1368	1621	838.9
	60^{th}	1821	1087	510.9
	80^{th}	2517	867.6	559.1
	100^{th}	2959	1003	513.3

References

1. Z. Wang, F. Qi, L. Yin, Y. Shi, C. Sun, B. An, H. Cheng and F. Li, *Adv. Energy Mater.*, 2020, **10**, 1903843.
2. W. Kuang, X. Zhou, Z. Fan, X. Chen, Z. Yang, J. Chen, X. Shi, L. Li, R. Zeng, J.-Z. Wang and S. Chou, *ACS Energy Lett.*, 2024, **9**, 4111–4118.
3. Wen, W. Fang, F. Wang, H. Kang, S. Zhao, S. Guo and G. Chen, *Angew Chem Int Ed*, 2024, **63**, e202314876.
4. Z. Lu, D. Liu, K. Dai, K. Liu, C. Jing, W. He, W. Wang, C. Zhang and W. Wei, Energy Storage Mater., 2023, **57**, 316–325.
5. N. Hong, J. Li, S. Guo, H. Han, H. Wang, X. Hu, J. Huang, B. Zhang, F. Hua, B. Song, N. Bugday, S. Yasar, S. Altin, W. Deng, G. Zou, H. Hou, Z. Long and X. Ji, *J. Mater. Chem. A*, 2023, **11**, 18872-18880.
6. W. Qin, Y. Liu, J. Liu, Z. Yang and Q. Liu, *Electrochim. Acta*, 2022, **418**, 140357.
7. N. Hong, J. Li, H. Wang, X. Hu, B. Zhao, F. Hua, Y. Mei, J. Huang, B. Zhang, W. Jian, J. Gao, Y. Tian, X. Shi, W. Deng, G. Zou, H. Hou, Z. Hu, Z. Long and X. Ji, *Adv. Funct. Mater*., 2024, **34**, 2402398.
8. W. Xu, R. Dang, L. Zhou, Y. Yang, T. Lin, Q. Guo, F. Xie, Z. Hu, F. Ding, Y. Liu, Y. Liu, H. Mao, J. Hong, Z. Zuo, X. Wang, R. Yang, X. Jin, X. Hou, Y. Lu, X. Rong, N. Xu and Y. S. Hu, *Adv. Mater.,* 2023, **35**, 2301314.
9. X. Liang, T.-Y. Yu, H.-H. Ryu and Y.-K. Sun, *Energy Storage Mater.*, 2022, **47**, 515-525.
10. Y. Lu, M. Song, J. Huang, L. Zhang, B. Zhao, W. Wu and X. Wu, *J. Energy Storage*, 2024, **77**, 109933.
11. K. Zhang, Z. Xu, G. Li, R. J. Luo, C. Ma, Y. Wang, Y. N. Zhou and Y. Xia, *Adv. Energy Mater.*, 2023, **13**, 2302793.
12. X. Dong, X. Wang, Z. Lu, Q. Shi, Z. Yang, X. Yu, W. Feng, X. Zou, Y. Liu and Y. Zhao, *Chin. Chem. Lett.*, 2024, **35**, 108605.
13. X. Meng, D. Zhang, Z. Zhao, Y. Li, S. Xu, L. Chen, X. Wang, S. Liu and Y. Wu, *J. Alloy. Compd.,* 2021, **887**, 161366.
14. Y. Fan, X. Ye, X. Yang, L. Guan, C. Chen, H. Wang and X. Ding, *J. Mater. Chem. A*, 2023, **11**, 3608-3615.